JOURNAL OF GEOPHYSICAL RESEARCH, VOL. 100, NO. C4, PAGES 6881–6898, APRIL 15, 1995

Turbulence variability at the equator in the central Pacific at the beginning of the 1991–1993 El Niño

R.-C. Lien,[1] D. R. Caldwell,[2] M. C. Gregg,[1] and J. N. Moum[2]

Abstract. A 38-day, 5990-cast microstructure study on the equator performed during the onset of the 1991–1993 El Niño shows the effect on small-scale activity at 140°W of an equatorial Kelvin wave. By using two ships, data were taken continuously from November 4 to December 12, 1991, near the National Oceanic and Atmospheric Administration Pacific Marine Environmental Laboratory mooring at 0°N, 140°W. The ships occupied the station sequentially with a 3.5-day overlap for intercalibration. Variability in currents was observed on tidal periods, and periods of 4 days (presumably equatorially trapped internal gravity waves), 8 days (cause unknown), 20 days (tropical instability waves), and longer (Kelvin waves). Variation in water structure occurred most prominently on the timescale of Kelvin waves. The diurnal cycle typical of that location was observed: nocturnal deepening of the surface mixed layer was accompanied by a "deep cycle," bursts of turbulence penetrating into the stratified region below the nighttime mixed layer. During the observational period, one Kelvin wave trough and one crest passed through the site. Changes accompanying the phase change in the Kelvin wave included a reversal of the near-surface current, a deepening of the thermocline, and a change of water mass. Changes in small-scale activity included a tenfold decrease of the thermal dissipation rate and a fourfold decrease of the rate of heat transport downward from the mixed layer. The nighttime mixed layer deepened from 30 to 60 m. The thickness of the stratified region in which nocturnal turbulence bursts occurred, the deep cycle region, thinned from 40 to 20 m because it was confined between the bottom of the nighttime mixed layer and the low-shear region near the core of the undercurrent. The decrease in downward heat flux observed at this passage of the downwelling Kelvin wave front could explain the rapid sea surface temperature (SST) increase seen at El Niño onsets. The magnitude of the change in vertical flux is similar to the magnitude of the change in horizontal advection. This process would produce a warmer SST much more quickly than could the advection of warm waters eastward.

1. Introduction

Because small-scale mixing of momentum and heat is crucially important to the dynamics of the equatorial current system [*Philander and Pacanowski,* 1980], a series of intensive microstructure expeditions was undertaken to the equatorial Pacific at 140°W in the 1980s. First, in November–December 1984, as part of the TROPIC HEAT experiment, simultaneous measurements were made by two groups on separate ships [*Chereskin et al.,* 1986; *Toole et al.,* 1987; *Peters et al.,* 1988, 1989; *Moum et al.,* 1989]. At this time the strong diurnal variability of turbulence near the equator was discovered, along with the "deep cycle" of bursts of turbulence that occurs nightly (when surface forcing is strong enough) between the base of the mixed layer and the core of the Equatorial Undercurrent (EUC) [*Moum and Caldwell,* 1985; *Gregg et al.,* 1985]. This deep cycle may be related to intensified high-frequency internal-wave activity at the base of the mixed layer [*McPhaden and Peters,* 1992; *Moum et al.,* 1992a,b; *Hebert et al.,* 1992]. A second set of cruises took place in March–April of 1987 [*Peters et al.,* 1991; *Hebert et al.,* 1991a,b]. Then, surface forcing was less intense than in 1984, the EUC was recovering from an El Niño event, winds were light, and turbulence was less intense.

One hypothesis that was tested on these cruises was the idea that turbulence is much stronger within a fraction of a degree of the equator than in surrounding waters [*Crawford and Osborn,* 1981]. Testing this hypothesis was complicated by strong temporal variability, especially diurnal, and by the ocean's response to vari-

[1]Applied Physics Laboratory, University of Washington, Seattle.

[2]College of Oceanic and Atmospheric Sciences, Oregon State University, Corvallis.

Paper number 94JC03312.
0148-0227/95/94JC-03312$05.00

ability in atmospheric conditions [*Moum et al.*, 1986; *Peters et al.*, 1989; *Hebert et al.*, 1991a]. It was concluded that turbulence is indeed enhanced, especially in the thermocline, but in a wider region, a region comparable in meridional extent to the extent of the EUC. Because of the complications, this result may not be clear in individual transects [*Hebert et al.*, 1991a].

Another puzzle was added by a calculation showing that vertical turbulent transport was not sufficient to close the zonal momentum budget in 1984 [*Dillon et al.*, 1989]. Was the missing momentum carried by internal waves? Is this process related to the deep mixing cycle? In 1987, turbulent transport was sufficient to close the budget [*Hebert et al.*, 1991b]. Is the difference between 1984 and 1987 due to the fact that surface forcing was much weaker in 1987? Is it related to the observation that the deep mixing cycle was weak in 1987?

In November–December 1991 the two groups returned to the site for the third time, as part of the "Tropical Instability Wave Experiment (TIWE)" to study the effects on turbulence and mixing of the 20- to 30-day tropical instability waves seen in satellite measurements of sea surface temperature [*Legeckis*, 1977], in currents [*Halpern et al.*, 1988], and in numerical model simulations [*Cox*, 1980].

Tropical instability waves are believed to be generated by an instability in the meridional shear of the equatorial currents [*Philander*, 1978]. They are usually strong in the northern hemisphere fall but tend to diminish with the onset of an El Niño [*Halpern et al.*, 1988]. (The expedition that furnished the data described herein took place a year after the large-scale portion of the TIWE was executed in the northern hemisphere fall of 1990.)

In 1991, to maintain a station long enough to observe two cycles of the tropical instability waves, two ships were used, *Wecoma* (Oregon State University group), and *Moana Wave* (University of Washington group). Each ship was on station at the equator at 140°W for 3 weeks, with a 3.5 day overlap period for intercalibrations [*Moum et al.*, 1994]. Thus a 38-day period was covered, from November 4 (Julian day 308) to December 12 (day 346), 1991. It turned out that tropical instability waves, which had been strong as usual at this time of year before our arrival at the equator, were suppressed during the observational period, which was coincident with the beginning of the El Niño of 1991–1993 [*McPhaden*, 1993].

A series of Kelvin waves propagated across the Pacific during the latter part of 1991 [*Kessler et al.*, 1995]. The passage of one of the strongest Kelvin waves through the site decreased the shear and stratification toward the latter part of the observational period. These changes in turn modified the small-scale physics. Because tropical instability waves were weak and the Kelvin wave was strong, the observations described herein recorded the response of the upper ocean to the passage of a Kelvin wave at the beginning of an El Niño to a greater extent than they recorded the ocean's response to tropical instability waves. In this paper we present the data obtained on these cruises, along with an attempt to connect the small-scale observations made on these and previous cruises with large-scale influences.

2. Normal Background Conditions at 140°W

Seasonal and interannual variations of surface winds, ocean temperatures, and currents on the equator at 140°W were documented by *McPhaden and McCarty* [1992] using Pacific Marine Environmental Laboratory (PMEL) long-term mooring measurements from 1983 to 1991. The surface wind stress is about 0.06 Pa in the boreal winter and about 0.04 Pa in the boreal spring and summer. The sea surface temperature (SST) is about 25°C in the boreal winter and about 26°C in the boreal summer. The dominant flows in the upper central equatorial Pacific are the South Equatorial Current (SEC) and the Equatorial Undercurrent (EUC). They are both seasonally modulated, as well as being modulated interannually by El Niño–Southern Oscillation (ENSO) events. The SEC flows westward in boreal winter but is replaced by an eastward flowing surface current in boreal summer. The eastward flowing EUC is stronger in boreal summer. In November and December the normal SEC flows westward at 0.2 m s^{-1} in the upper 40 m and the normal EUC flows eastward with a speed of about 1 m s^{-1} with its core at 120 m depth.

In years with no El Niño, tropical instability waves superimpose meridional velocities much larger than the mean on the current pattern. For example, although the 1983–1991 mean meridional current was less than 0.04 m s^{-1} southward in the upper 50 m, superimposed on it in 1990 were 20-day meridional current oscillations greater than 0.4 m s^{-1}.

3. Background Conditions at 140°W, June 1990 to June 1992

In the boreal fall of 1990 the surface wind stress was about 0.07 Pa, slightly stronger than its climatological mean (Plate 1). SST varied between 25°C and 26°C. The SEC flowed westward in the upper 60 m, and the EUC declined in strength from its summer intensity. The meridional velocity showed six cycles of 20- to 30-day tropical instability waves in the upper 100 m with an amplitude about 0.4 m s^{-1} (Plate 1).

In the spring and summer of 1991, wind stress, SST, and currents repeated their normal non-ENSO seasonal cycles; the wind stress decreased slightly, SST increased to about 28°C, the SEC was replaced with an eastward flowing current, the EUC increased its intensity, and the tropical instability wave disappeared.

In the boreal fall of 1991, however, the normal non-ENSO cycle did not continue. Although SST decreased as usual until the middle of September, it then rapidly increased from 25°C to 28°C. The SEC appeared between July and mid-September accompanied by two cycles of tropical instability waves. But in September,

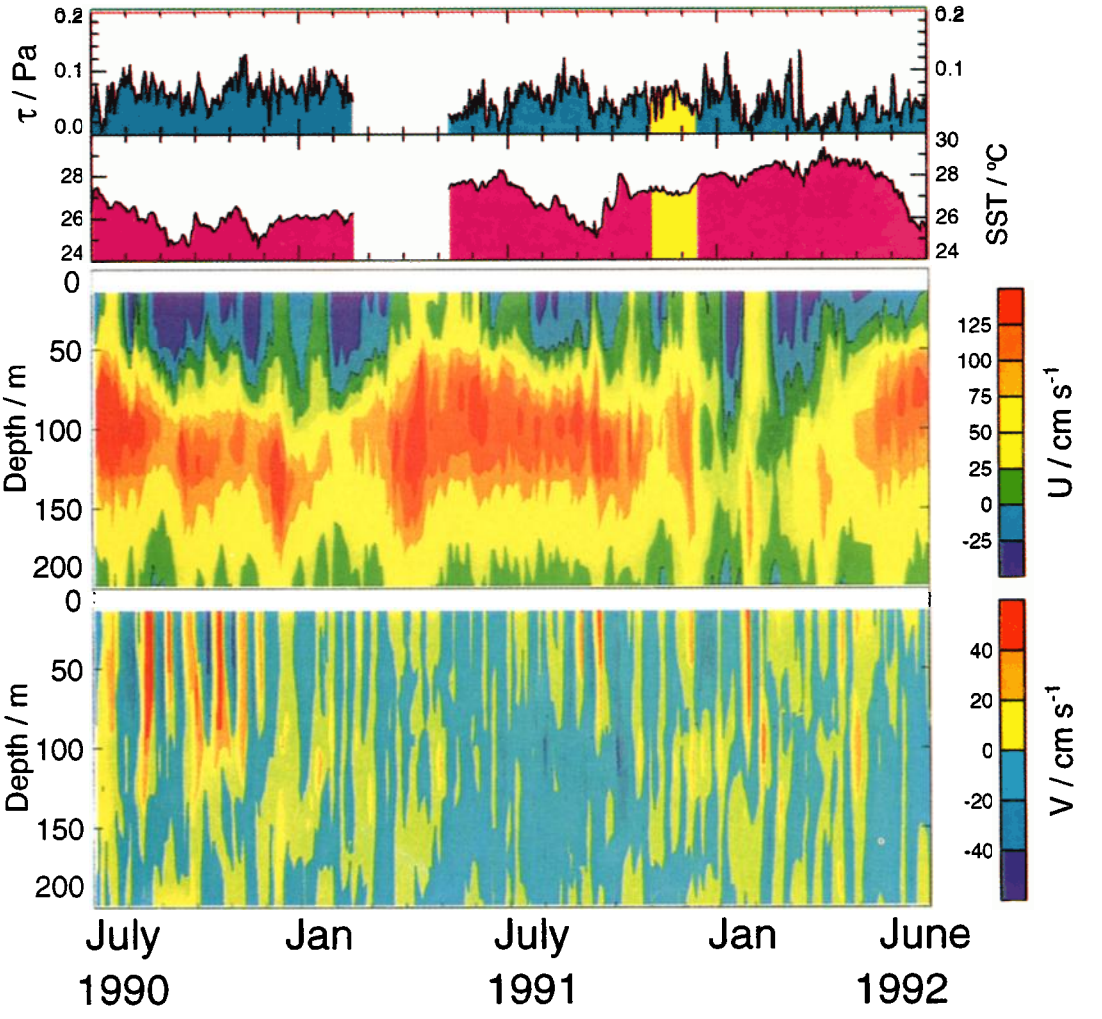

Plate 1. (top to bottom) Long-term plots of surface wind stress, sea surface temperature (SST), zonal currents with eastward velocities positive, and meridional currents with northward velocities positive. Tropical instability waves appear as vertical red markings which denote large northward current. The period of Tropical Instability Wave Experiment (TIWE) small-scale measurements is denoted by the yellow sections of the wind stress and SST. These data were taken by the mooring maintained by the National Oceanic and Atmospheric Administration (NOAA) Pacific Marine Environmental Laboratory (PMEL) at 0°N, 140°W [*McPhaden,* 1993]. Currents were measured with an acoustic Doppler current profiler (ADCP).

surface current flowed eastward and the tropical instability waves were suppressed while the SST rose. The eastward speed of the EUC dropped to less than 0.25 m s^{-1} in December 1991 and in February 1992.

Both the abnormal SST and the current anomalies were associated with the 1991–1993 El Niño [*McPhaden,* 1993]. During the El Niño onset, four Kelvin waves, identified by the depression of 20°C isotherm depths, crossed the Pacific (Plate 2). The constant-phase line indicates that their origin lay in the western Pacific (W. S. Kessler, personal communication, 1994). At 140°W the 20°C isotherm depths increased from 120 m to more than 160 m during the passage of the second and third Kelvin waves. Our measurements began in the trough following the first wave and extended past the crest of the second. (At the "crest" of a Kelvin wave the thermocline is depressed and wave currents flow eastward at the surface [*Ramage,* 1986].)

4. Measurements

Wecoma was on station from November 4–25 (days 308–329), *Moana Wave* from November 21 to December 12 (days 325–346). A schematic diagram (Figure 1) shows the platforms and measurements.

Measurements from *Wecoma* included the following: (1) Microstructure temperature, conductivity, and shear in the upper 200 m, using the profiler CHAMELEON. (2) Current measurements from a ship-mounted 153 kHz acoustic Doppler current profiler (ADCP). (3) Meteorological measurements from a suite of instruments aboard ship, e.g., air temperature, humidity, shortwave, and long-wave radiation, SST, and winds. (4) High-frequency current measurements from a sideways-looking ADCP hanging 35 m below the ship. (5) High-frequency temperature measurements recorded by two thermistor chains, one hung from the bow and the

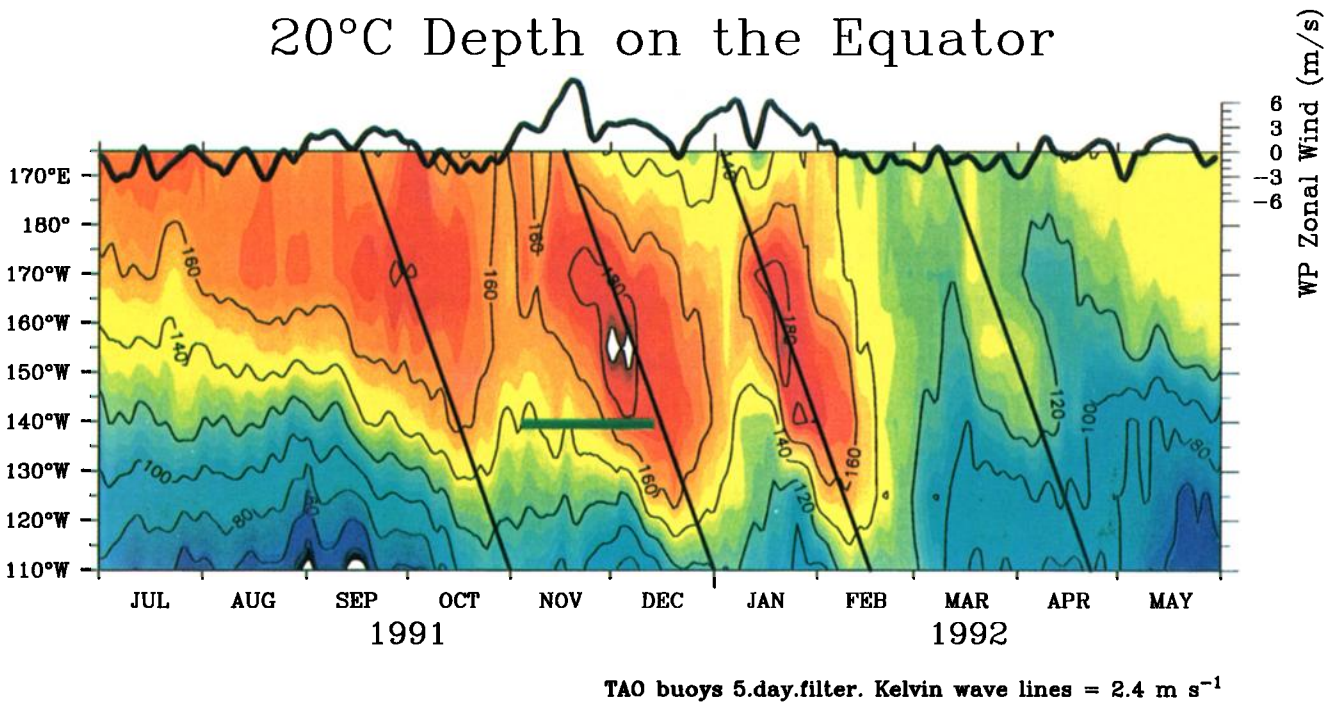

Plate 2. The depths of the 20°C isotherm across the equatorial Pacific during the onset of the 1991 El Niño. The thick solid curve on top of the contour represents the zonal wind speed at 165°E. The horizontal green box indicates the longitude and time of the TIWE measurements. The tilted lines mark constant phase lines of Kelvin waves. (Courtesy of W. Kessler)

other hung near the stern (M. D. Levine and J. N. Moum, Detailed observations of an equatorial internal-wave packet, submitted to *Journal of Physical Oceanography*, 1995).

Measurements made from *Moana Wave* included the following: (1) Microstructure temperature, conductivity, and shear in the upper 200 m, using the Advanced Microstructure Profiler (AMP). (2) Current measurements from a ship-mounted 153 kHz ADCP. (3) Meteorological measurements from a suite of instruments mounted on a special tower constructed on the bow, e.g., air temperature, humidity, short-wave, and long-wave radiation, SST from a tube floating on the ocean surface, wind, and precipitation. Also, atmospheric profiling was performed [*Chertock et al.*, 1993].

To provide a context of longer-term measurements, the ships stayed near the long-term National Oceanic and Atmospheric Administration (NOAA) PMEL mooring at the site. The mean distance from the buoy to *Wecoma* was 3 km; to *Moana Wave*, 3.6 km. The maximum distance from the buoy to *Wecoma* was 10 km; to *Moana Wave*, 8.4 km. Besides its normal long-term measuring capability, the mooring was outfitted with a fast responding thermistor string.

A total of 3918 CHAMELEON casts and 2072 AMP casts was made. Rather than attempt to maintain a fixed schedule for casts, the maximum amount of data was obtained by releasing the instruments to descend again immediately after each recovery as long as they were working satisfactorily. (This procedure is safer for the instruments than holding them near the surface or bringing them on deck.) Because of the occasional necessity of repairs and delays caused by other operational difficulties, the resulting time series of profiles was an unevenly sampled one.

The turbulent kinetic energy dissipation rate ε was estimated by the usual method of sensing small-scale shears from the freely falling profilers. Because of the importance of this quantity, a careful comparison of ε estimated by the two groups during the 3.5-day overlap period (November 21–25, days 325–329) was conducted. It revealed no systematic bias between the measurement systems, although short-term differences caused by the natural spatial variability of the ocean did appear [*Moum et al.*, 1995].

During earlier experiments at this site, profiling was limited to the region above the EUC core (about 120 m) because cable drag in the strongly sheared currents slowed descent and caused strong vibrations [*Peters et al.*, 1988]. During TIWE, two modified AMP profilers were used which easily penetrated below the EUC core. Instrumental noise due to the vibration of the profilers' hulls was moved out of the signal band. Modification of CHAMELEON allowed it also to profile usefully below the core.

The ADCP measurements were described in detail by *Lien et al.* [1994]. The vertical resolution for velocity was approximately 7 m for *Wecoma* measurements and approximately 4 m for *Moana Wave*. The resolutions for shear were 14 m and 8 m, respectively.

From *Wecoma*, surface fluxes were estimated by bulk formulas. From *Moana Wave*, surface wind stress and latent and sensible heat fluxes were estimated by one of three methods, the covariance method, the inertial

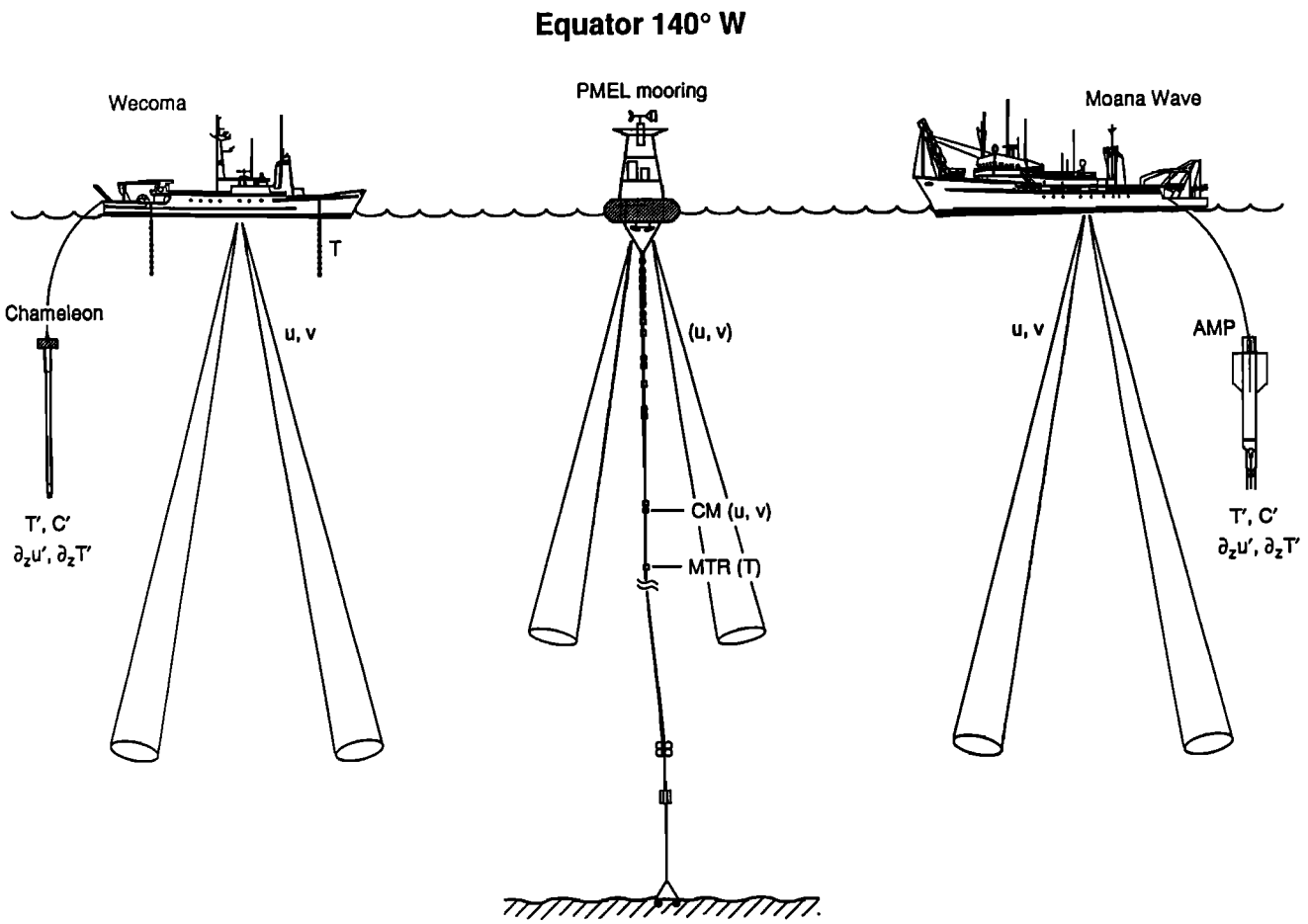

Figure 1. TIWE experiment and measurements. Oregon State University (OSU) measurements were taken from R/V *Wecoma*, and University of Washington measurements were taken from R/V *Moana Wave*. The current meters and MTRs are part of the NOAA/PMEL long-term mooring.

dissipation method, and bulk formulas. At times when all three methods produced good data, the median of the three estimates was used.

To simplify some of the analysis, data were grouped by hours and averaged. For example, the data from all microstructure casts within 1/2 hour of each hour were averaged. For only 41 hours out of a total of 915 hours were there no casts available. Individual profiles were used in calculations for which error might be introduced by the hourly averaging process, the calculation of heat flux out of the mixed layer, for example.

5. Surface Forcing and Large-Scale Ocean Conditions, November/December 1991

5.1. Atmospheric Conditions During the Microstructure Station

Both air and sea surface were warmer by 2°C than climatological means, with diurnal variations of 0.5°C in the air and 0.3°C in SST (Figure 2). The wind remained southeasterly and easterly throughout. The average wind stress, 0.07 Pa, was comparable to the monthly mean at this location and season. Spectra of the wind stress and its components showed dominant variance at frequencies smaller than 0.01 cph (not shown). Variability in the zonal component was about three times greater than variability in the meridional component. There was no significant diurnal variation of the wind stress. At night the surface buoyancy flux was dominated by the latent heat flux.

5.2. Currents and Shear

During the experiment, both the SEC and the EUC showed significant variations (Plate 3). Between November 4 and 16 (days 308–320) the EUC flowed at 0.8 m s^{-1}, less than its climatological mean (1.0 m s^{-1}). Its core was at 120 m depth. The speed of the SEC was similar to its climatological mean. The EUC accelerated to more than 1 m s^{-1} between November 24 and December 4 (days 328–338), and the westward flowing SEC disappeared. Between December 5 and 11 (days 339–345) the EUC core became vertically diffuse and the surface current flowed eastward at a speed of 0.4 m s^{-1}.

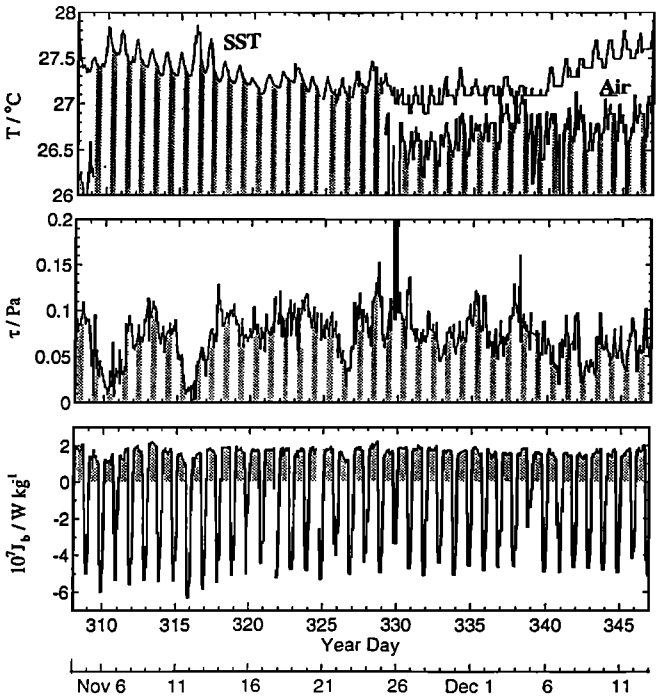

Figure 2. Meteorological measurements during the period of small-scale measurements. (top) Air temperature (not available between days 310 and 324 because of a sensor malfunction) and "sea surface" temperature (SST). From day 308 to day 328 the sea surface temperature measurements were taken at about 1 m depth (from the *Wecoma*), whereas for the remainder of the period the sea surface measurements were taken by a sensor floating on the sea surface (from the *Moana Wave*). (middle) Wind stress. (bottom) Total buoyancy flux, including short-wave and long-wave radiation and latent and sensible heat fluxes. Times of local darkness are indicated by the solid stripes on the plots.

The most prominent peak in meridional velocity spectra had a 4-day period (Figure 3). Four-day oscillations might be related to the equatorially trapped inertial gravity waves first identified in sea level records [*Wunsch and Gill,* 1976]. In the upper layer the spectral level of the meridional velocity at 20-day period may be related to tropical instability waves. The 4-day and 20-day waves have rms amplitudes of 0.1 to 0.2 m s^{-1}. Peaks seen at periods of 20, 8, and 4 days in the upper layer zonal velocities are not significant. Both components show significant peaks at diurnal and semidiurnal frequencies. The rms amplitudes for diurnal and semidiurnal tides are 0.03–0.04 m s^{-1} at all depths. Isotherms and isopycnals were displaced semidiurnally by 10–20 m (Plate 5).

The vertical shear was dominated by its zonal component, except near the EUC core (Plate 4). The average shear in the zonal current was about 0.02 s^{-1} (log (shear) = -1.7) above the EUC core between November 4 (day 308) and December 1 (day 335), but it decreased to less than 0.01 s^{-1} (log (shear) = -2) after that. The depth of the strongest vertical shear fluctuated in unison with the depth of the core of the EUC. Typically, the meridional component of shear was less than 0.01 s^{-1}. Above the EUC core the total vertical shear was greater than 0.02 s^{-1} during the period November 4 (day 308) to December 1 (day 335), but it decreased by a factor of about 2 after December 1.

5.3. Manifestation of the Kelvin Wave at 140°W

Several characteristics of a Kelvin wave can be used in its identification. Its "crest" can be identified by the maximum depression of the thermocline and a maximum in its eastward zonal currents, which can cause eastward currents at the surface [*Ramage,* 1986]. Its trough can be identified by a maximum in the near-surface westward current. (At its crest a Kelvin wave reduces the vertical shear in the upper layer, by superposing its positive shear on the negative shear of the EUC.)

At the start of our observation period the Kelvin wave was in its "trough" phase at 140°W. The zonal flow in the upper (20–60 m depth) ocean was westward, the thermocline lay at 120 m depth, and a relatively low-salinity (35.0) water mass occupied the site (Figure 4). During the following 30 days the 20- to 60-m zonal current first turned eastward, then accelerated until it reached its eastward maximum of 0.6 m s^{-1} on day 338. The thermocline (marked by the 24°C isotherm) deepened throughout this period, especially rapidly from day 332 to day 338. This sequence of events is consistent with the nature of Kelvin waves [*Johnson and McPhaden,* 1993]. On day 340 a different water mass arrived which by day 343 on the 22.77 σ_θ surface had a salinity of 35.3, an increase of 0.3 in 3 days (Figure 4). The crest (days 338–339) is identified on Figure 4. The trough is not as well defined, but probably passed near day 313, when the westward current in 20- to 60-m depths reached its maximum.

5.4. Temperature, Salinity, and Density

In November–December 1991, SST was warmer (27°C) than its usual winter value (25°C). Between December 5 and 12 (days 339 and 346) the average temperature in the upper 100 m increased again, by 0.5°C (Plate 5). This warming was likely caused by the Kelvin wave bringing a different water mass into the region. The thermocline depth increased from 120 to 180 m.

The salinity had a complicated temporal and vertical structure. High-salinity layers seemed to move vertically with the thermocline and the EUC core as before [*Chereskin et al.,* 1986]. A tongue of salinity greater than 35.5 appeared occasionally (Plate 5), possibly by meridional advection of a high-salinity tongue typically located south of the equator [*Wyrtki and Kilonsky,* 1984].

The density field displayed features similar to those of the temperature field. The pycnocline deepened from 120 m before November 27 (day 331) to about 180 m after December 4 (day 338). The EUC core seemed to follow the 23.50 isopycnal surface until the core became too diffuse for its identification. (In November–

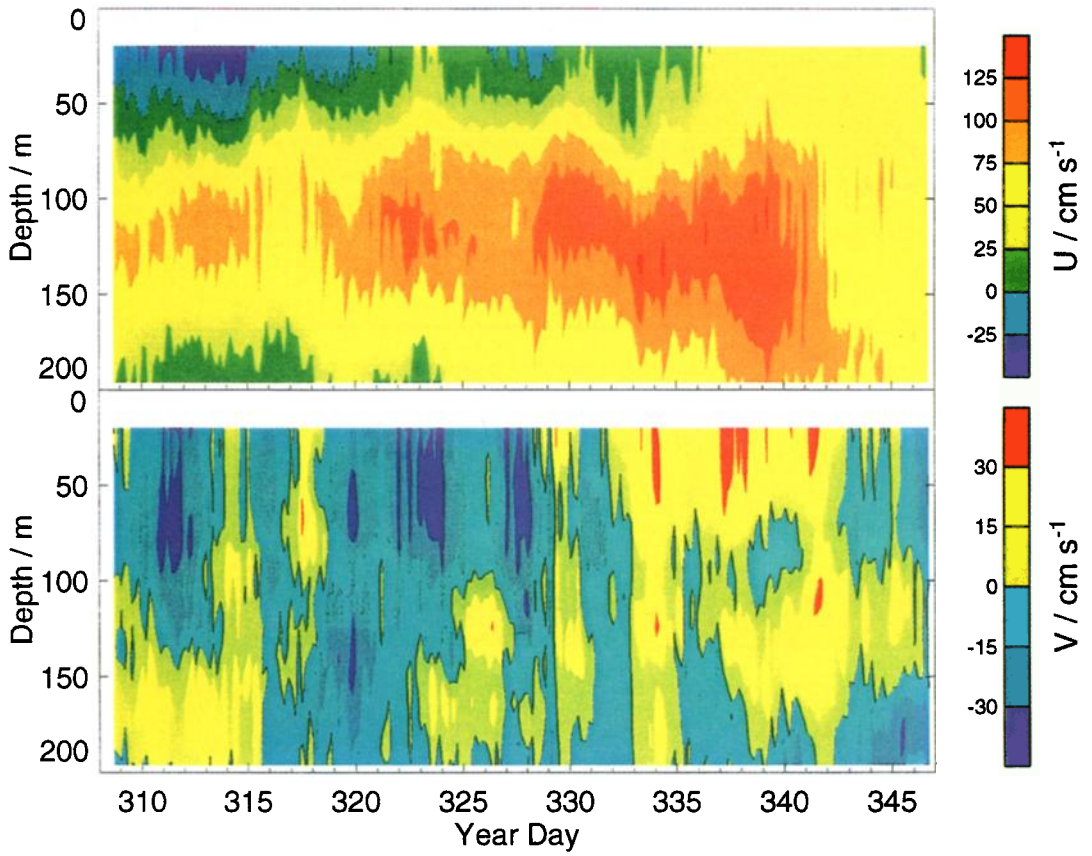

Plate 3. (top) Zonal and (bottom) meridional components of currents measured by ADCP from the ships during the experimental period. Positive zonal velocity is eastward; positive meridional velocity is northward.

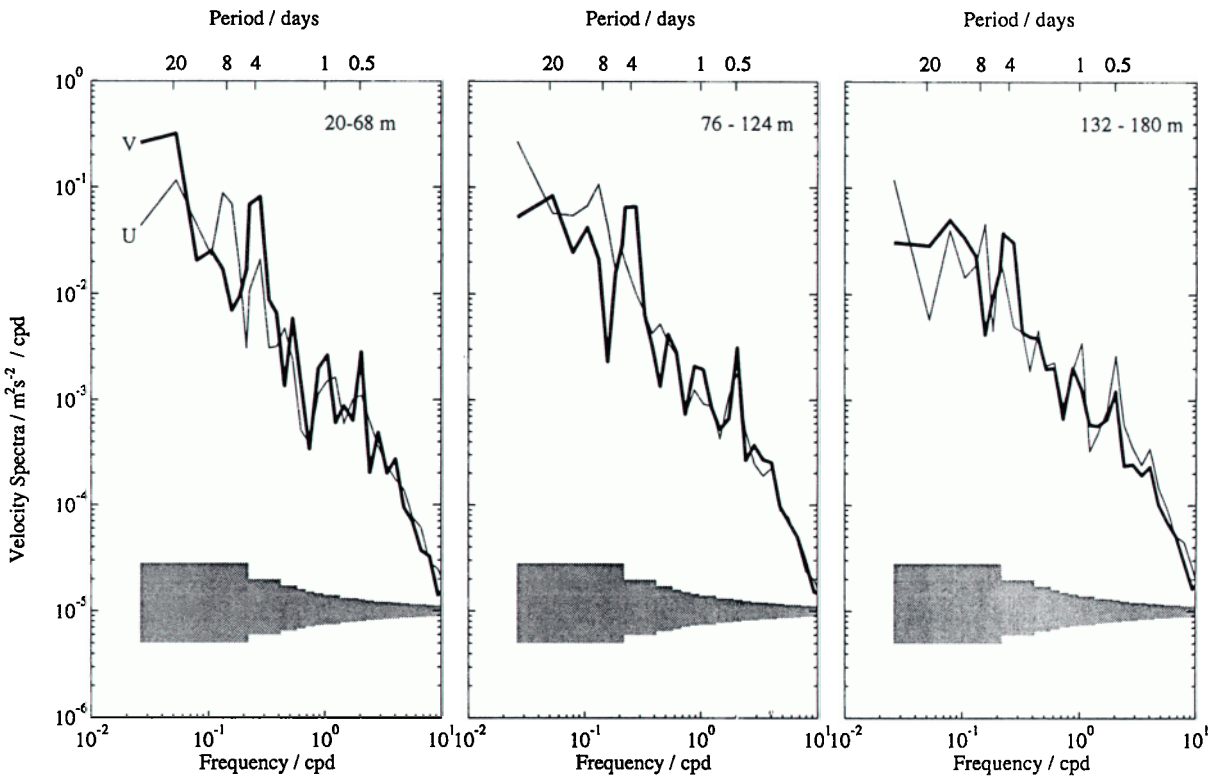

Figure 3. Spectra of velocity components averaged over three depth ranges. The zonal components are indicated by thin lines, meridional components by thick lines. The 95% confidence limits are shown as shaded at the bottom of each plot.

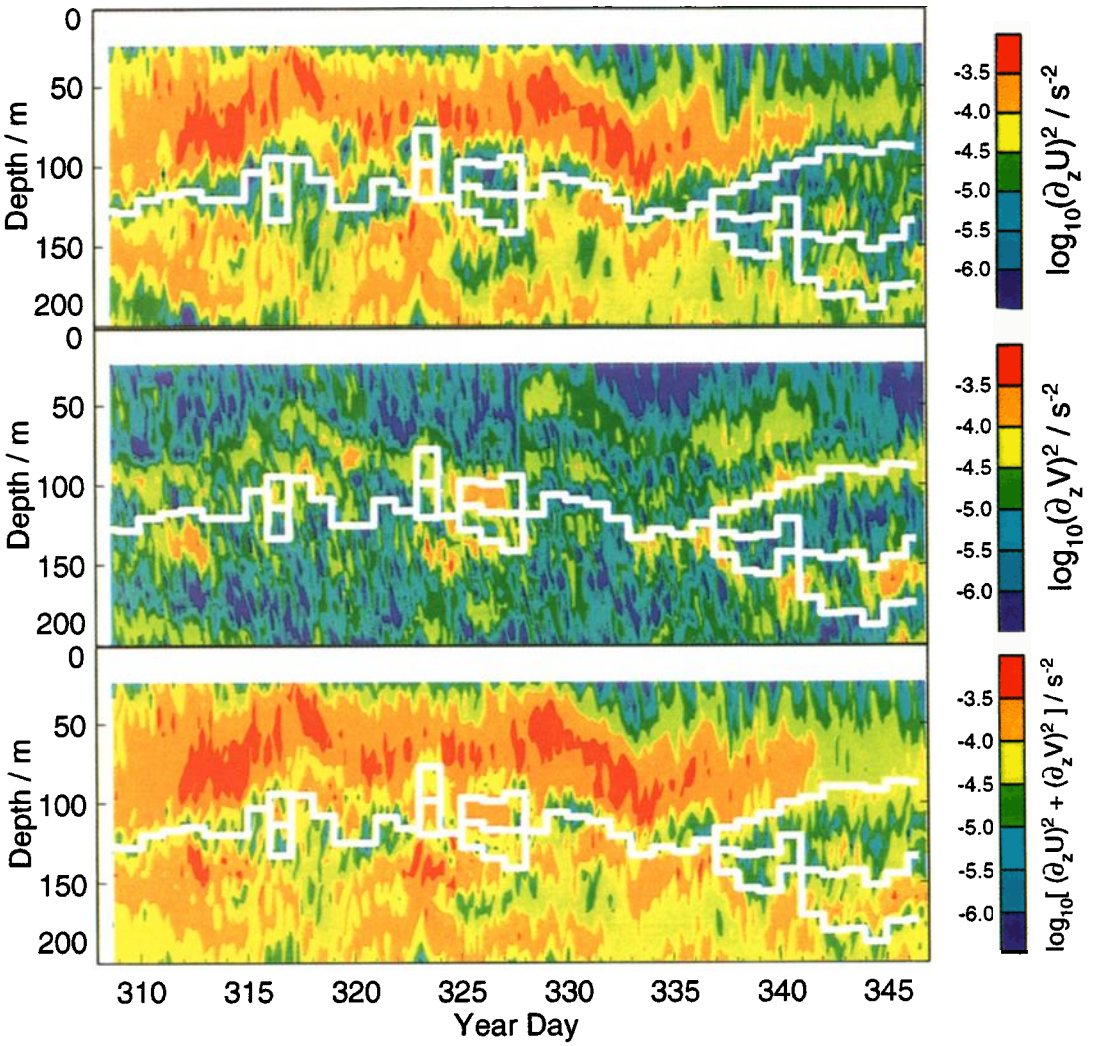

Plate 4. Contours of logarithms of shear-squared measured by ADCP from the ships. (top) Vertical shear-squared in the zonal current. (middle) Vertical shear-squared in the meridional current. (bottom) Total shear-squared. The white lines represent daily means of the depth of the undercurrent core.

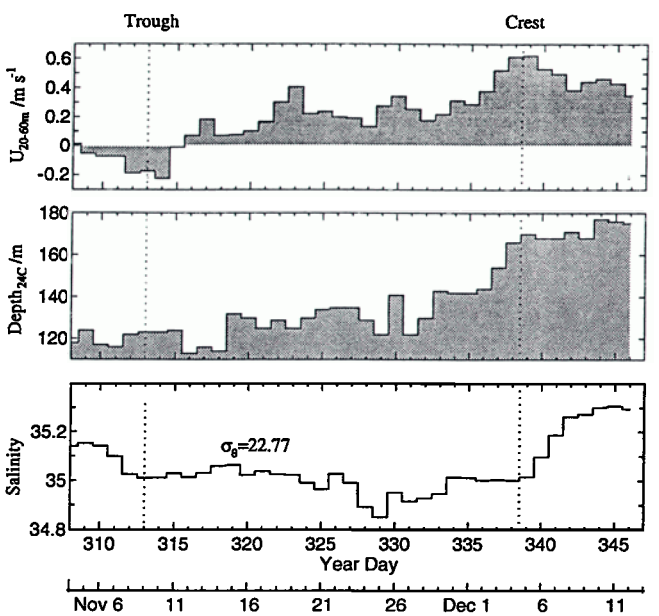

December 1984 the core followed the 25.25 isopycnal surface [*Chereskin et al.*, 1986]. In April 1987 the core of the undercurrent followed the 24.0 isopycnal for several days and then switched to the 25.5 isopycnal for 10 days [*Peters et al.*, 1991].)

5.5. Surface Mixed-Layer Depth

Following *Peters et al.* [1988] and *Moum et al.* [1989], we define the surface mixed-layer depth to be the depth at which the density exceeds its surface value by 0.01 kg m^{-3}. By this definition the daytime mixed-layer depth ranged from 7 to 20 m (Plate 6). The nighttime mixed-layer depth varied between 15 and 40 m before November 27 (day 331) and then became deeper than 60 m after November 28 (day 332).

Figure 4. Manifestations of the Kelvin wave. Daily averages of (top) zonal current averaged from 20 to 60 m depth, (middle) depth of the 24°C isotherm, and (bottom) salinity at the depth where $\sigma_\theta = 22.77$.

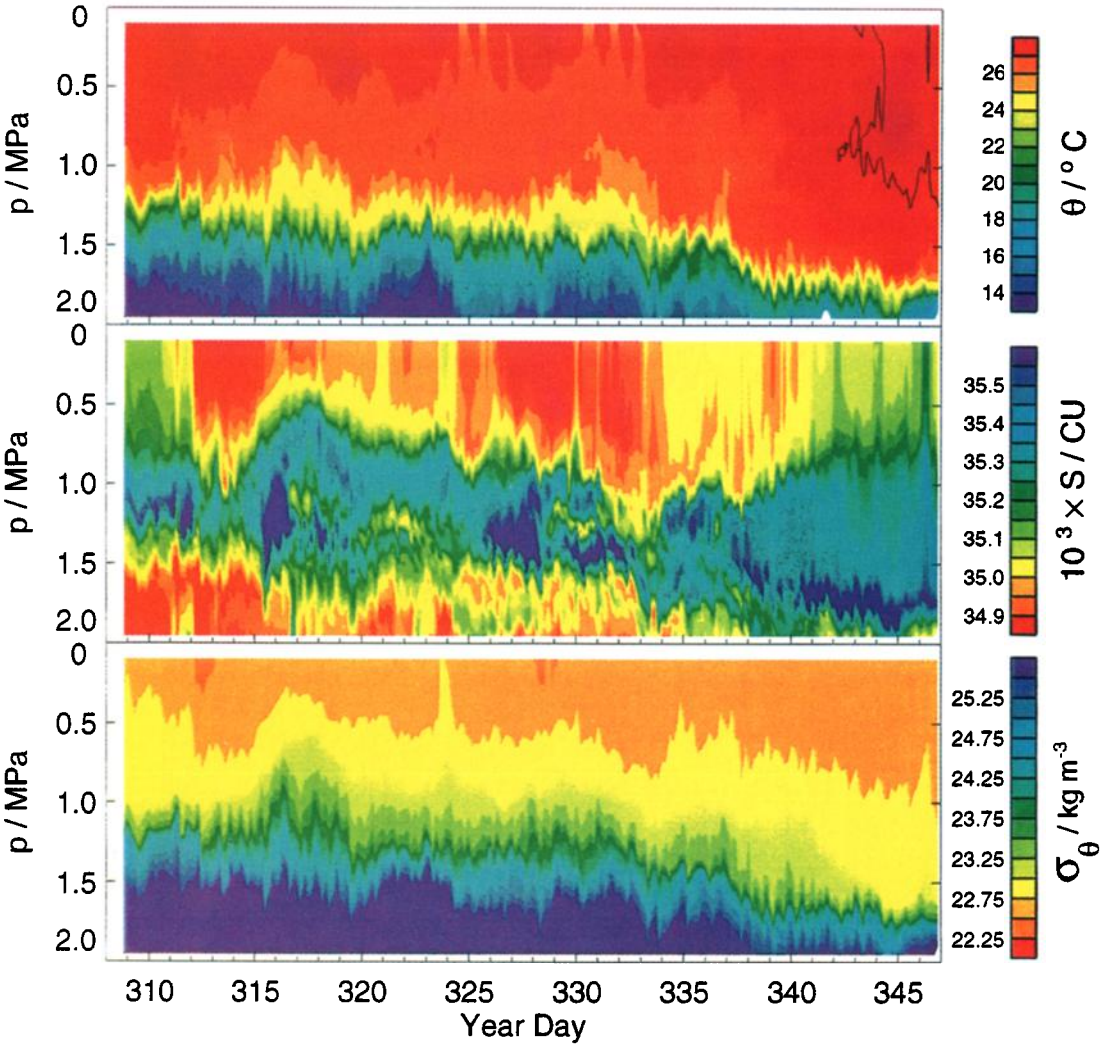

Plate 5. Contours of (top) temperature, (middle) salinity, and (bottom) σ_θ during the measurement period. The solid black line in the temperature plot represents the 27.5°C isotherm.

5.6. Stratification, Shear, and Richardson Number

Within the depth of penetration of the nighttime surface mixed layer, both shear and stratification varied diurnally (Plate 6 and Figure 5). As the mixed layer deepened in the nighttime, shear and stratification decreased as the water was mixed. When the nighttime convection ceased at daybreak, the water was restratified by solar heating and, perhaps, upwelling of the background stratification and lateral advection. The shear is restored, presumably by the large-scale pressure gradient and the wind stress.

Does the Richardson number show a diurnal variation also? In 1984 it appeared not to, at least in the 10- to 25-m depth range [*Chereskin et al.*, 1986]. In their observations, the buoyancy frequency N and shear varied diurnally in phase so that their ratio, the Richardson number, remained constant. *Peters et al.* [1989, p. 18,007], addressing observations made at the same time concluded that "contrary to *Chereskin et al.* [1986], we found a clear, although not entirely regular, diurnal variation in the 10–25 m Ri." In the present data, at depths of 20–28 m, for example, where the mixed layer is present for a considerable portion of the time (Figure 5, top), the morning solar warming increases N before the shear is restored, a tendency that is most easily seen on days 335–347 (Figure 5). Before that time the nighttime mixed layer did not consistently penetrate past 28 m, so ADCP shear measurements are not available. In the depth range 20–28 m the diurnal cycle in both N and shear can be seen easily. The shaded area indicates stability in the sense that the Richardson number is greater than one fourth. When the shading is missing, the Richardson number is one fourth or smaller and turbulence is to be expected. Periods of stability occur in the morning at 20–28 m because the shear is slower to re-establish itself after the nighttime mixing than the stratification. This situation holds to 44 m. Below 44 m the diurnal cycle is indistinct and the morning periods of stability are not seen.

In terms of the Richardson number, the above conclusions mean that in the present data *Ri* varied diurnally at depths reached by the nighttime mixed layer.

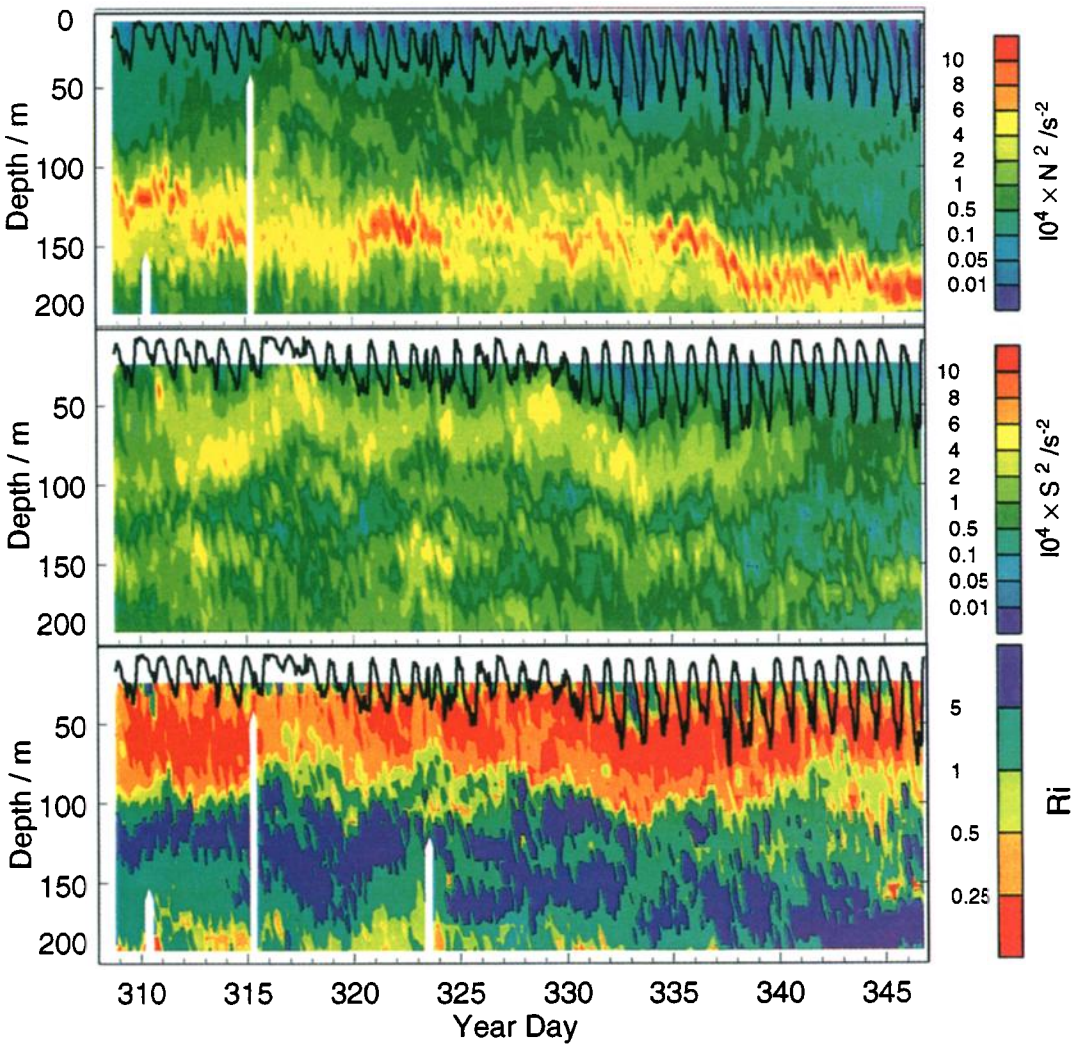

Plate 6. Contours of (top) N^2 derived from microstructure instruments, (middle) shear-squared from the ships' ADCPs, and (bottom) Richardson number calculated from these values for N^2 and shear-squared. The solid black lines represent the mixed-layer depth, defined as the depth at which σ_θ exceeds its surface value by 0.01.

It seems that different processes are responsible for the restoration of the shear than those responsible for the restratification.

On days 336–346 the water in the deep cycle depth range is almost always unstable, although some periods of stability are seen at the end of the period as the shear weakens (Figure 5). Below 80 m the flow is stable nearly all of the time in this period. The effect of the Kelvin wave on the stability is easily seen at 80 m depth where the water was mostly unstable before day 340 and stable afterward. The effect of the Kelvin wave in decreasing the shear had more effect on the Richardson number than the decrease in N in the new water mass.

6. Turbulence and Mixing

Measurements of ε showed large diurnal variations in the upper 100 m, not only within the mixed layer, but also in the stratified water below (Plate 7). Within the surface mixed layer, vigorous mixing at night produced values of ε greater than 10^{-7} W kg^{-1}, whereas in the daytime, ε did not exceed 10^{-8} W kg^{-1} in the restratified water. The one exception occurred on day 329, which had the deepest daytime mixed layer and a daytime mixed-layer ε that remained as strong all day as it had been the previous night. This loss of diurnal variation was probably caused by the combination of a weak wind at night and a strong wind during the day.

Immediately below the nighttime mixed layer the shear was large enough to reduce the Richardson number below 1/4 most of the time (Plate 6). At night, bursts of turbulence penetrated through this region below even the nighttime mixed layer, sometimes as deep as 90 m (Figure 6). This deep cycle turbulence was seen most often in bursts of 2–4 hours duration. Dissipation in this stratified layer was sometimes stronger than it was in the mixed layer and often persisted past daybreak. These bursts of turbulence are very similar to those first found in 1984 in this location [*Gregg et al.*, 1985; *Moum and Caldwell*, 1985].

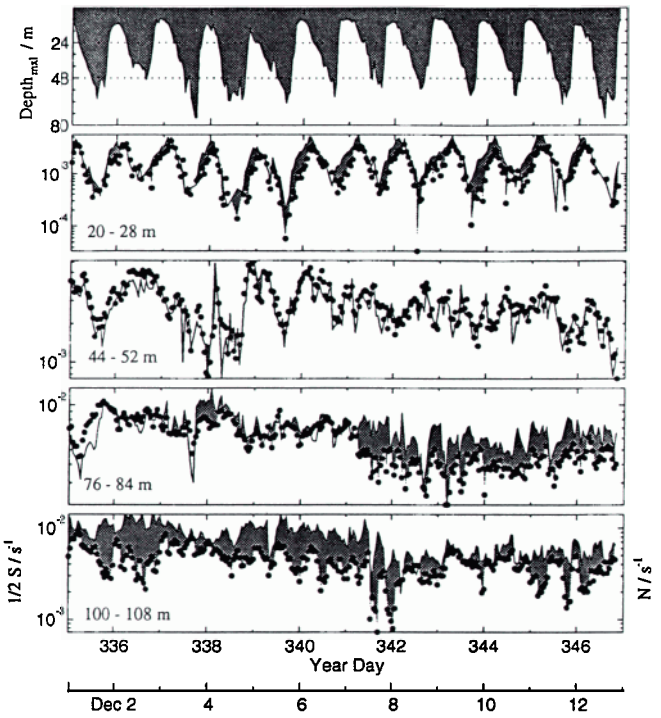

The coefficient of correlation between nighttime mixed-layer depth and deep cycle penetration depth was 0.6 (95% confidence level 0.3). However, the deep cycle depth did not increase as much as the mixed-layer depth, so on nights with deep mixed layers the deep cycle range was thinner because the deep cycle is restricted to the high-shear region above the EUC core.

Detailed examination of ε in each of the different vertical regimes (Figure 7) shows the diurnal variation and the penetration of mixing into the stratified water. In the part of the mixed layer below 15 m depth, vertically averaged estimates of ε (Figure 7a) are large at night, average values above 10^{-7} W kg^{-1} being quite common. (Daytime estimates of ε in this region are mostly not available because the mixed layer retreated above 15 m most days.) The solid line in Figure 7a represents val-

Figure 5. Time series of N (solid lines) superimposed on shear-squared (solid circles) on a logarithmic scale at various depths. In the top panel the mixed-layer depth ($\Delta\sigma_\theta = 0.01$) is shown. When N^2 exceeds 1/4 shear-squared, the region between the two is shaded to indicate a stable condition.

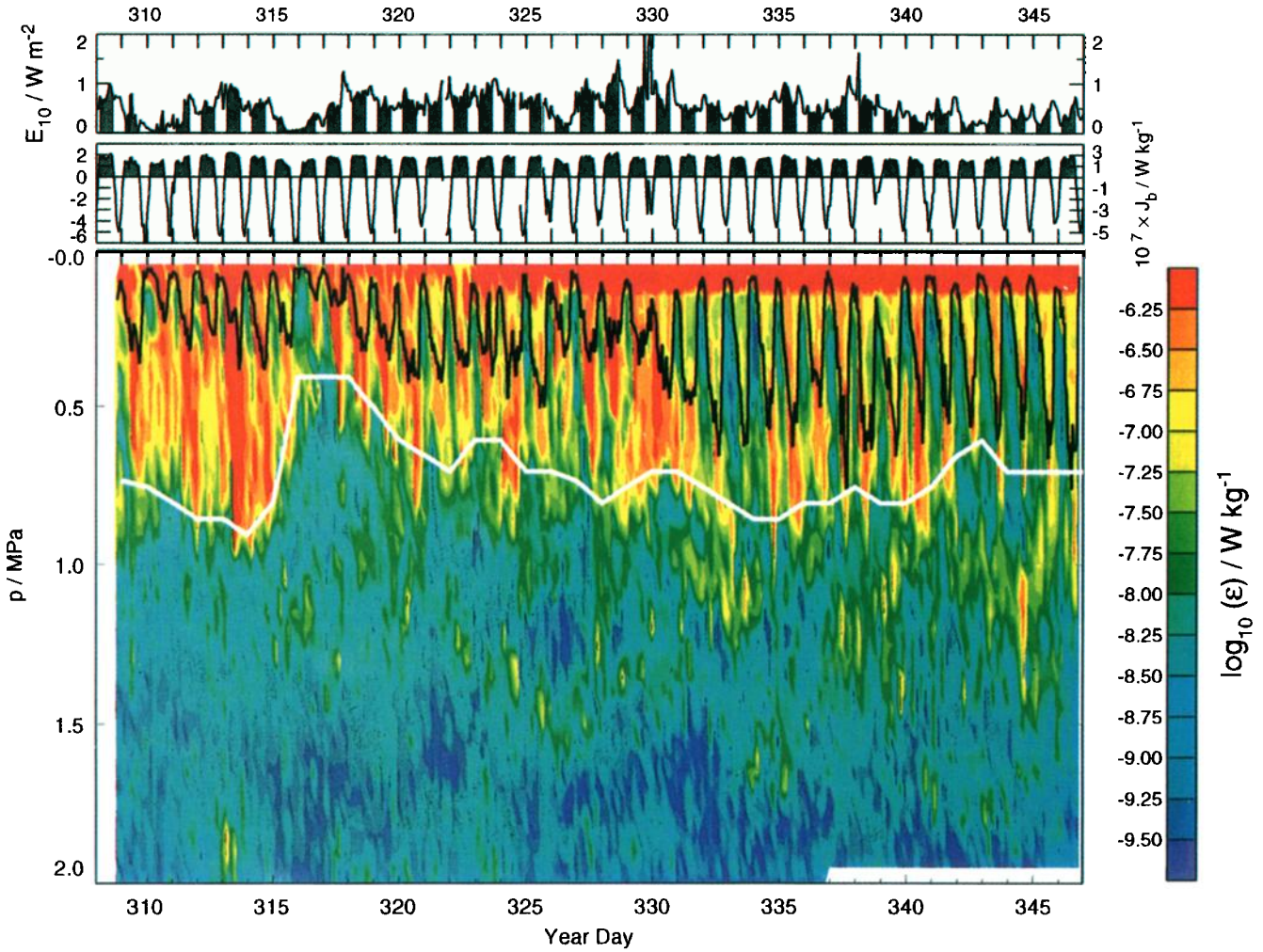

Plate 7. Contours of logarithms of the turbulent kinetic energy dissipation rate ε. Above the ε plot are time series of the 10-m wind power and the buoyancy flux. The mixed-layer depth is indicated by the black line on the contour plot. The depth above which the Richardson number is 1/4 is indicated by the white line.

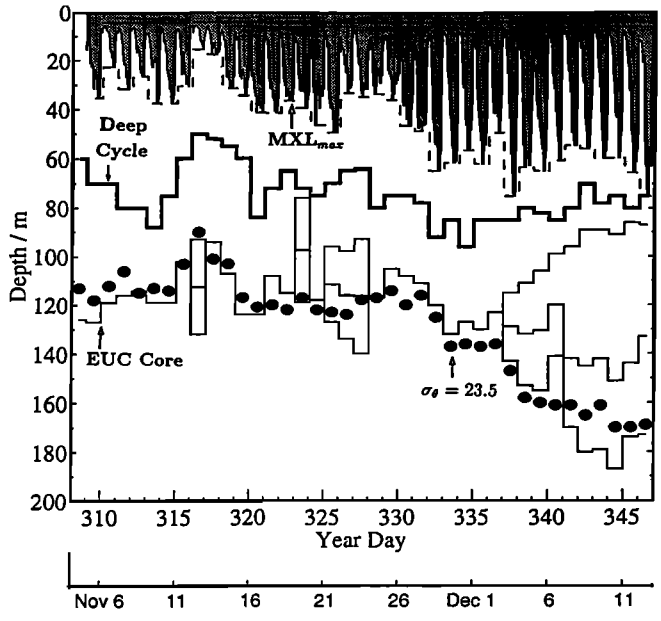

Figure 6. Daily averaged depths of mixed layer (dashed line), deep cycle (thick solid line), Equatorial Undercurrent (EUC) core (thin solid line), and isopycnal surface of $\sigma_\theta = 23.5$ (solid circles). The mixed layer region defined by hourly data is shaded. (At times, the depth of the EUC core cannot be unambiguously defined.)

ues of ε calculated by using a similarity scaling, based on the surface wind stress and buoyancy flux, which has succeeded in midlatitudes [*Lombardo and Gregg*, 1989]. Discrepancies between observations and similarity scaling have been found previously at the same location [*Peters et al.*, 1989; *Moum et al.*, 1989]. These authors suggested that the discrepancies may be due to the shear-driven turbulence generated by the mean shear of the undercurrent. (Mean shear is not considered in this similarity scaling.) This view is supported by the fact that the measured ε exceeds the predicted ε in the first part of the observation period when the shear is strong but agrees better in the latter part of the period when the shear has diminished. However, this scaling ignores also the potentially large role of surface waves in turbulence generation near the surface [*Anis and Moum*, 1994].

In the always stratified region between the nighttime mixed layer and the penetration depth of the deep cycle (Figure 7b), ε is approximately as large as it is in the mixed layer. It has been speculated that this turbulence is caused by internal waves propagating downward from the mixed layer. It has also been speculated that the deep cycle is caused by shear instabilities [*Moum et al.*, 1992a].

Between the bottom of the deep cycle and the core of the undercurrent, (Figure 7c), ε was a factor of 10 smaller, with no diurnal variability. In a 10-m band centered on the EUC core (Figure 7d), ε was smaller yet, especially near the beginning of the period. Below the EUC, to 200 m depth, ε rarely exceeded 10^{-8} W kg^{-1}, with no periodicity (Figure 7e).

Strong thermal dissipation rates χ of about 10^{-7} °C^2 s^{-1} were found mostly in the following three places: (1) in the thermocline, (2) near the base of the mixed layer, and (3) in the deep cycle. The diurnal variation of χ was not as strong as the diurnal cycle of ε. Events of strong thermal dissipation often accompanied a strong deep cycle.

The Cox number, $3\langle(dT'/dz)^2\rangle/(\langle dT/dz\rangle)^2$, closely related to the eddy diffusivity for heat by the Osborn-Cox relation $K_h = \kappa \times$ Cox number (κ is the molecular

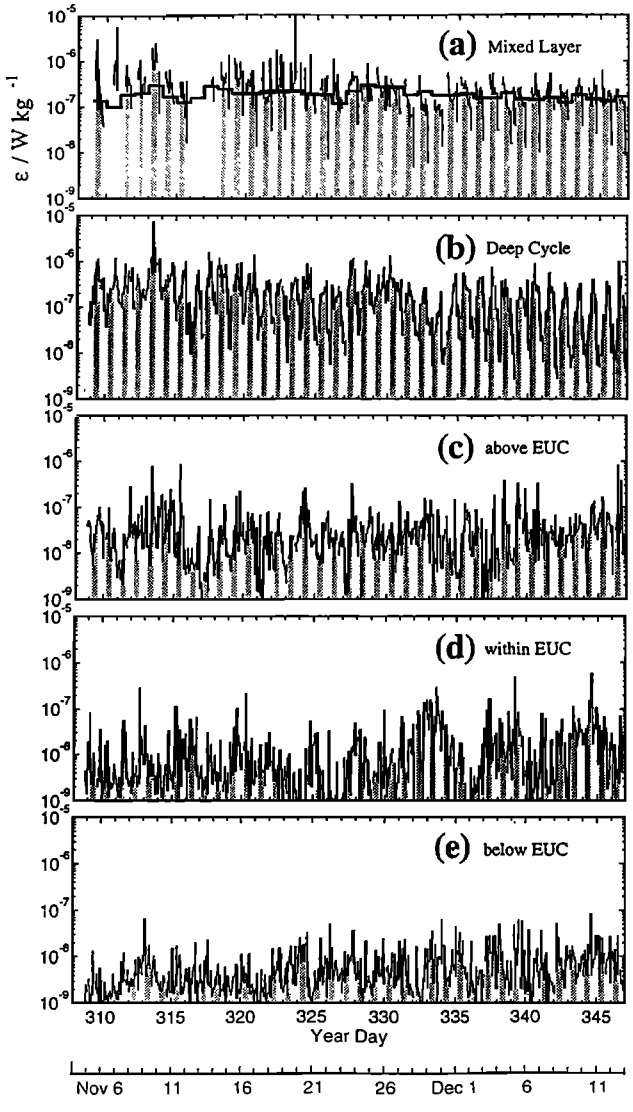

Figure 7. Time series of ε averaged over various depth ranges. (a) 15 m depth to the depth of the mixed layer. (Daytime values are not available because the mixed layer usually retreated above 15 m in the daytime.) The scaling of *Lombardo and Gregg* [1989] is represented as a thick black line on this panel. (b) Between the nighttime mixed layer and the penetration depth of the deep cycle. (c) From the penetration depth of the deep cycle to 5 m above the core of the undercurrent (the precise depth of the bottom of this region was defined operationally as 5 m above the $\sigma_\theta = 23.5$ isopycnal). (d) A 10-m thick vertical band centered on the EUC core ($\sigma_\theta = 23.5$). (e) 5 m below the core of the undercurrent ($\sigma_\theta = 23.5$) to 200 m.

diffusivity), has large values in the mixed layer, in the deep cycle, and occasionally deeper in the water column (Plate 8). It does not decrease at the crest of the Kelvin wave as χ does but, rather, increases at most depths.

7. Effect of the Kelvin Wave on Turbulence and Vertical Fluxes

If we assume that the major background influences on turbulence and mixing are the energy supplied by the local wind and the phase of the Kelvin wave, we look for correlations on a plot of daily averages (Figure 8). To show temporal variations of the wind forcing, the 10-m height wind power is plotted on Figure 8a. To indicate the phase of the Kelvin wave, we plotted the near-surface (20–60 m) zonal current U_{20-60} in the bottom. Dissipation, averaged from 20 to 100 m is plotted on Figure 8b. The correlation between ε_{20-100} and E_{10} is not strong (correlation coefficient 0.26, just at the 95% confidence level), and there is no obvious correlation between ε and the Kelvin wave phase. (The correlation between ε averaged from 10 to 110 m, the averaging used by *Moum and Caldwell* [1985], and E_{10} is 0.46, significant well beyond the 99% confidence level, 0.35.) In this average the Cox number changes little, but averages over this depth range tend to be dominated by mixed-layer numbers. The turbulent heat flux downward from the mixed layer's base J_h (Figure 8d) shows similar correlation with E_{10} (0.31) but begins to decrease rapidly at the crest of the Kelvin wave. The dissipation of temperature variance χ, averaged from 20 to 100 m, also decreases rapidly at the crest of the Kelvin wave.

Using Figure 8 for guidance, we select two periods to compare small-scale parameters before and after the crest, days 315 to 330 as an example of the before-crest period and days 341 to 346 as an after-crest sample. Between the two periods the stratification in the upper 160 m decreases (Figure 9a). At the same time, the total shear-squared dropped by a factor of 3 or so (Figure 9b). The net effect on the Richardson number in the upper 80 m is a reduction at some depths (Figure 9c).

Comparison of ε and χ profiles before and after the passage of the crest of the Kelvin wave (Figures 9d and 9e) shows a decrease in ε in the upper 60 m by a factor

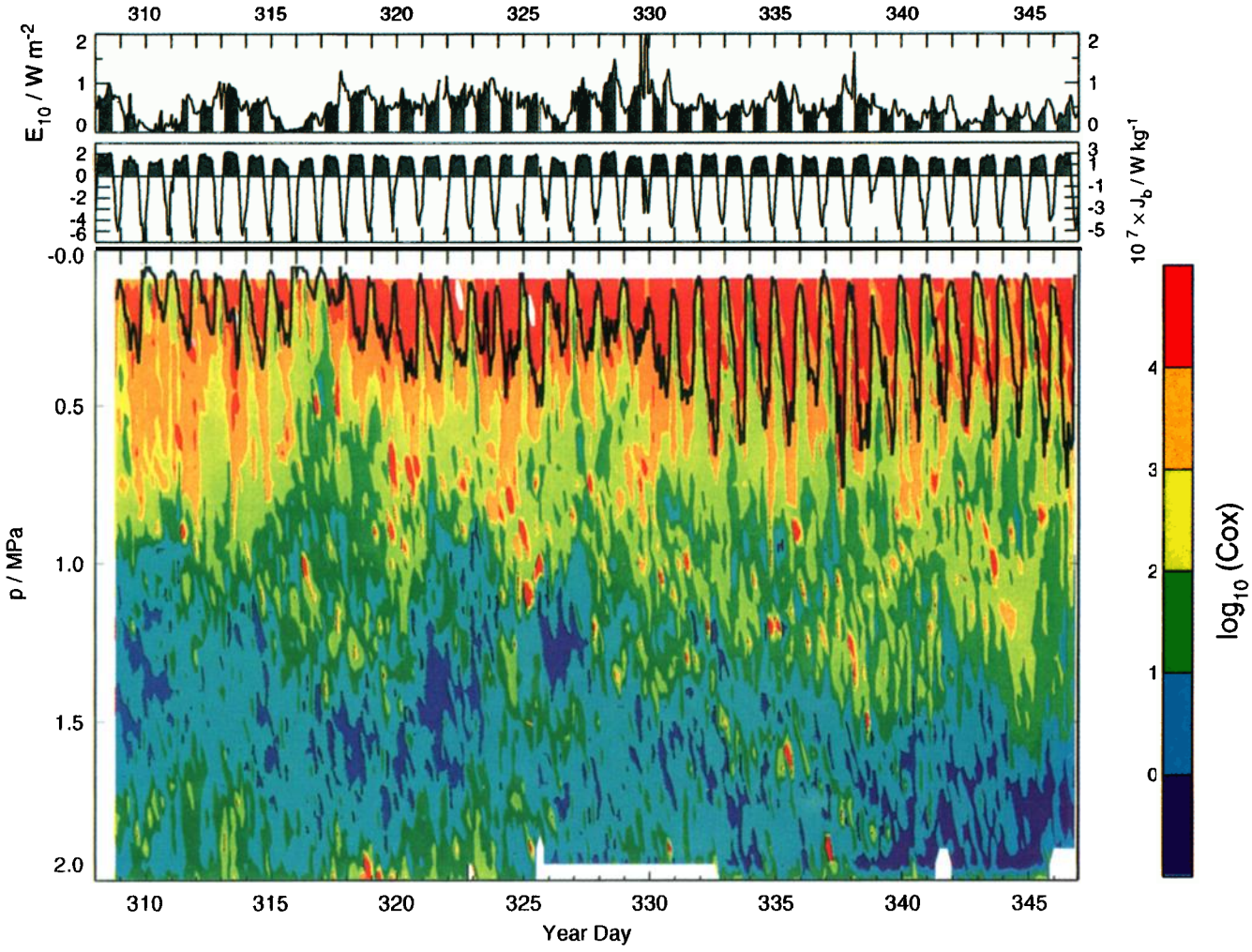

Plate 8. Contours of logarithms of the Cox number. Above the contour plot are time series of the 10-m wind power and the buoyancy flux. The hourly mixed-layer depth is represented by a black line on the Cox number plot.

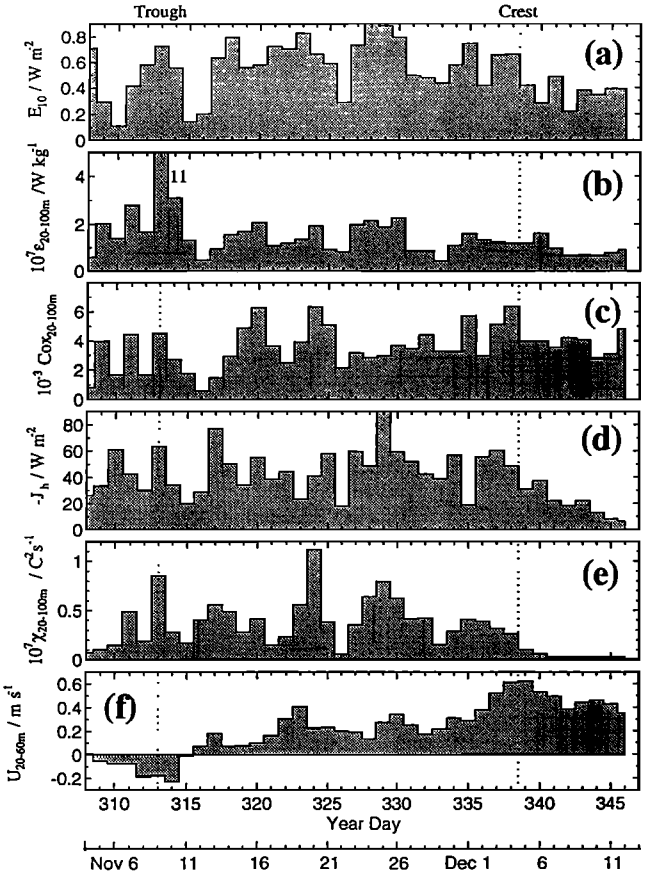

Figure 8. Daily averages of (a) 10-m wind power, (b) ε averaged between 20 and 100 m, (c) the Cox number averaged from 20 to 100 m, (d) the heat flux transported downward from the base of the surface mixed layer, (e) χ averaged between 20 and 100 m, and (f) the zonal velocity component averaged from 20 to 60 m. On day 313, the average value of ε was 11×10^{-7}, off scale. The 1-m-averaged vertical heat flux was calculated for every microstructure cast. The eddy diffusivity was calculated following *Osborn* [1980], with the mixing efficiency taken as 0.2. The vertical heat flux between the base of the mixed layer and 5 m below it was averaged to represent the heat flux out of the surface mixed layer. The turbulence momentum flux was calculated as $J_m = -K_m dU/dz$, the eddy viscosity being estimated by the dissipation method using dissipation rates and ADCP shear averaged for 1 hour in time and 8 m in depth.

of 2. The decrease in χ was even greater, more than a factor of 10. The Cox number increases at most depths.

Comparing vertical transports before and after the crest of the Kelvin wave, we see that the estimated eddy coefficient for momentum K_m increased by a factor of 4 in the whole range, to 200 m (Figure 10a). The eddy coefficient for mass K_ρ increased at most depths also (Figure 10b). The increase of eddy coefficients below 80 m depth at the crest of the Kelvin wave was due to the stronger turbulence dissipation rate and weaker shear and stratification.

The zonal and meridional components of turbulence momentum transports decreased nearly linearly with depth in the upper 80 m (Figures 10c and 10d). The zonal component remained the same after the crest of the Kelvin wave as it had been during the trough. The meridional component was twice as strong during the crest.

Before the crest, turbulence had been transporting heat downward at all depths, at rates ranging from 50 W m^{-2} at 20 m to less than 10 W m^{-2} below 60 m. As the crest passed, this transport weakened because the vertical temperature gradient weakened. At depths between 30 and 80 m, the turbulence actually transported heat upward because of the temperature inversion in this (salinity-stratified) depth range. The downward heat flux from the mixed layer to the stratified water below decreased from 40 W m^{-2} to less than 10 W m^{-2} after the crest of the Kelvin wave passed. (Figure 8c).

8. Comparison With 1984 and 1987

For the three periods for which we now have intensive turbulence measurements at 140°W on the equator, (1) November–December 1984, (2) March–April 1987, and (3) November–December 1991, large-scale conditions and local surface forcing were quite different.

1. In November–December 1984, typical November conditions prevailed. Local wind forcing was strong (0.07 Pa), as were instability waves. In response, the mixed layer was fairly deep (20–30 m), there was a deep cycle below the mixed layer in which the Richardson number was near 1/4, the deep cycle was intense, and downward transport of heat in the 20- to 80-m depth range was strong (60 W m^{-2} downward [*Moum et al.*, 1989]). Turbulence in the depth range 10–110 m was well correlated with the wind during a 12-day station [*Moum and Caldwell*, 1985].

2. In March–April 1987, the system was recovering from an El Niño and the EUC was weak. Wind forcing was also weak (0.02 Pa), as expected this time of year, and large-scale waves were not present. The result was a shallow mixed layer (10–25 m), with larger Richardson numbers below it, a weak deep cycle, and much less vertical heat transport (10 W m^{-2} downward).

3. In November-December 1991, as described herein, an El Niño was beginning, instability waves were absent, and strong Kelvin waves were passing through the site. Observations commenced near the trough of a Kelvin wave and ended just after the crest. Local surface forcing was large as in 1984 (0.07 Pa). The mixed layer was even deeper than in 1984 (30–60 m), the deep cycle was strong again, and the vertical heat transport was almost as strong as in 1984 (40 W m^{-2} downward), until the last week of observations, after the crest of the Kelvin wave arrived, when it decreased to less than 10 W m^{-2}.

We speculate as follows: What is the difference between these periods that causes the differences in heat flux? The conditions for each are listed in Table 1.

1. For November 1984 versus November 1991, conditions are quite similar, if the absence of Kelvin waves has the same effect as the presence of a Kelvin wave midway between its crest and trough, except that in

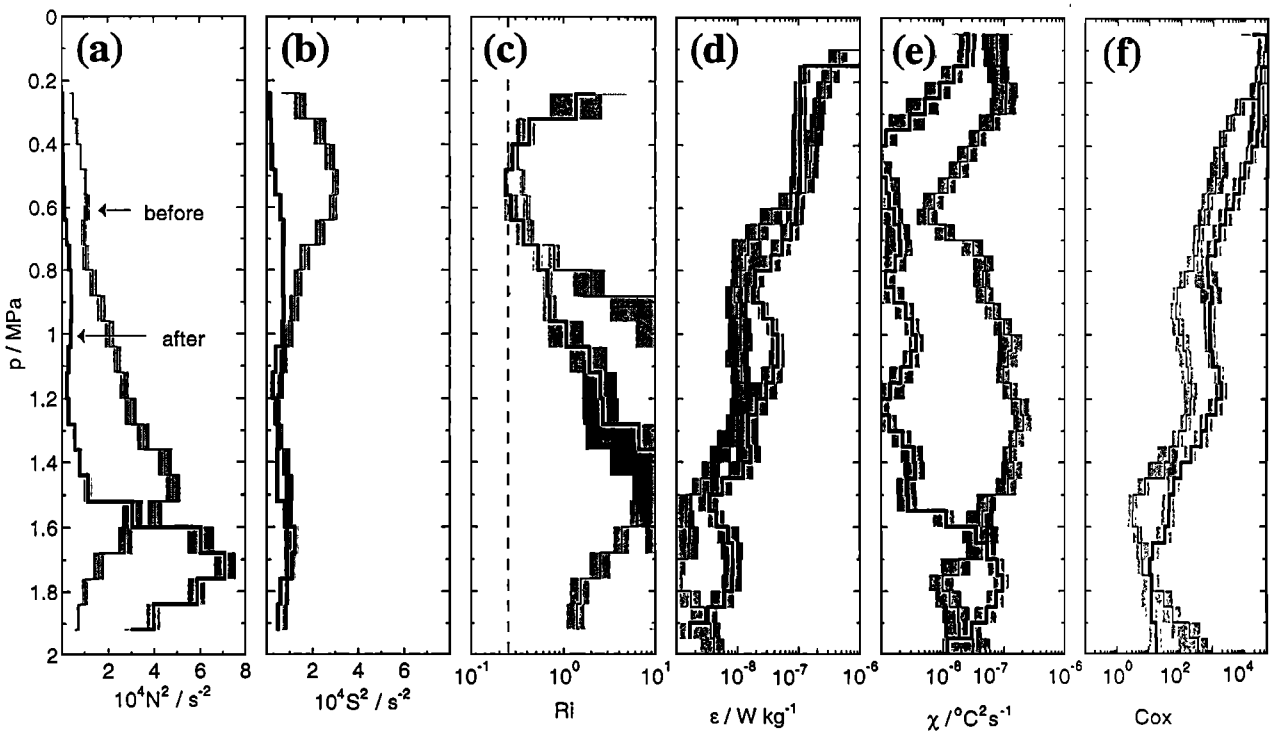

Figure 9. Mean profiles of (a) N^2, (b) shear-squared, (c) Richardson number, (d) ε, (e) χ before (thin line) and after (thick line) the peak of the Kelvin wave, and (f) Cox number. The period before was taken as days 315 to 330, the period after was taken as days 341 to 346. The 95% confidence limits are indicated by the shading.

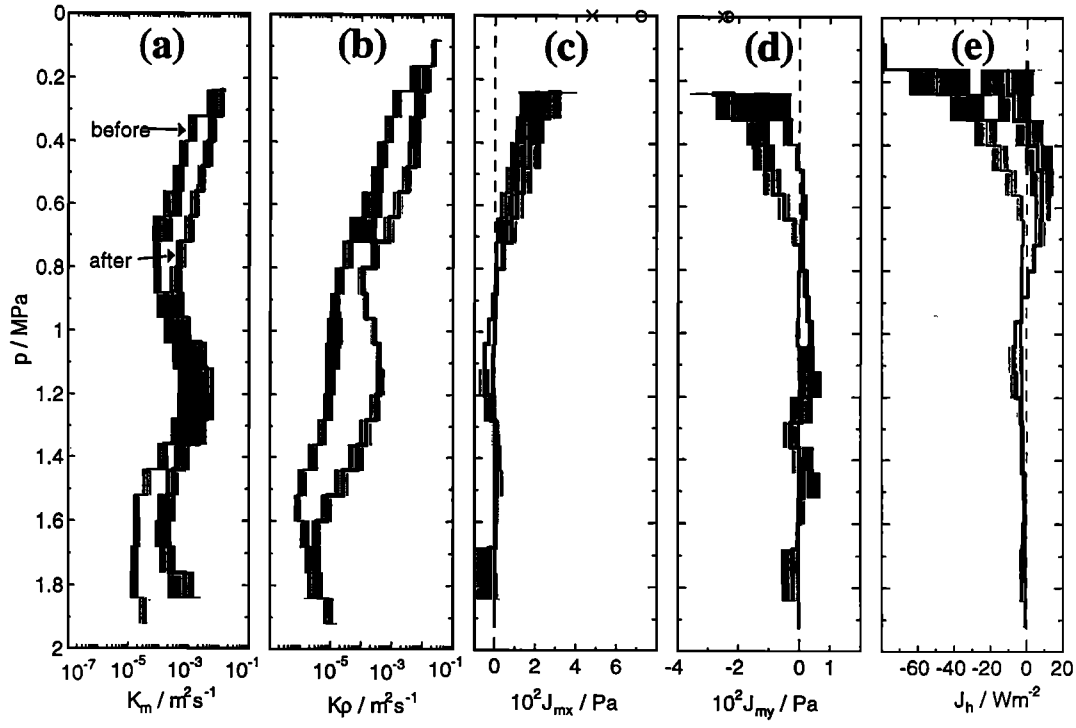

Figure 10. Mean profiles of eddy coefficients of (a) momentum K_m and (b) mass K_ρ, the vertical turbulent transports of (c) zonal momentum J_{mx} and (d) meridional momentum J_{my}, and (e) the vertical turbulent heat transport J_h. The time periods are the same as for Figure 9. The thin line represents an average from day 315 to day 330, intended to represent conditions before the crest of the Kelvin wave arrived. The thick line represents an average from day 341 to day 346, intended to represent conditions as the Kelvin wave crested. The 95% confidence limits are indicated by shading.

Table 1. Comparison of Various Equatorial Observations at 140°W

	Nov. 1984	April 1987	Nov. 1991	Dec. 1991
Wind	strong	weak	strong	strong
Instability waves	strong	weak	weak	weak
Kelvin waves	absent	absent	midlevel	crest
Shear	strong	weak	strong	weak
Stratification	moderate	strong	moderate	weak
Deep cycle	strong	weak	strong	weak
Heat flux from mixed layer	60 W m^{-2}	10	40	10

1984 the tropical instability waves were strong, whereas in November of 1991 they were weak. The heat fluxes were similar. We might conclude that the tropical instability waves did not profoundly affect the vertical heat flux in these cases. (In weak zonal flow and strong tropical instability waves we might expect these waves to influence turbulence.)

2. For November 1984 versus December 1991, if tropical instability waves are not a major influence on heat flux, as we "concluded" above, then the major difference between these two periods is the Kelvin wave cresting in December 1991. The heat flux is much smaller in December 1991. We might conclude that the cresting of the Kelvin wave has a significant influence in reducing the heat flux, even in strong winds.

3. For November 1984 versus April 1987, if the instability waves do not severely affect the heat flux, as concluded in comparison 1, then the only difference is the wind. The heat flux was much larger in 1984 when the wind was much stronger, so we could conclude that the local wind increases the heat flux significantly.

The conclusions reached in the house of cards constructed above are that the wind strengthens the heat flux, the Kelvin wave's crest weakens it, and tropical instability waves do not have a dominant effect. We advance this argument as a working hypothesis for future study, not as a strongly supported conclusion.

9. Conclusions

Hydrography and currents at 0°N, 140°W vary on many timescales. These are not only the diurnal and the typical timescales of atmospheric forcing, but also 4 days (presumably equatorially trapped internal gravity waves), 20 days (tropical instability waves), and longer (Kelvin waves). Sometimes variability is dominated by one or two of these, and their effects can be seen clearly. For example, in November 1984 the deep cycle part of the diurnal signal was strong, whereas in April 1987 the deep cycle was weaker by a factor of 2 [*Peters et al.*, 1994]. In the boreal fall of 1990 the tropical instability waves were strong, whereas on the cruises described in this paper the waves were weak. In the period of the 1991, 38-day station the effects of phenomena at the various periods of variability were of the same order, making the separation of their effects difficult.

The effect of the cresting Kelvin wave at the 140°W site on the near-surface water was to increase the SST, weaken the vertical shear, and deepen the thermocline. A new water mass was brought into the region in a short time. At the same time, the core of the undercurrent was vertically diffused and its speed was reduced. The effects of these changes on the turbulence and mixing were the following:

1. The nighttime surface mixed layer deepened from 30 to 60 m, even though the surface wind stress and nighttime cooling convection decreased. (The mean wind stress before the Kelvin wave trough was 0.075 ± 0.007 Pa (95% confidence limits), during and after the crest of the Kelvin wave the mean wind stress was 0.058 ± 0.005 Pa.) This deepening was probably caused by the weakening of both background stratification and equatorial upwelling.

2. Despite the reduction of shear-squared and stratification by a factor of 4 (Figure 9) a layer of subcritical Richardson number consistently remained below the surface mixed layer, although its thickness decreased as the mixed layer deepened.

3. Bursts of turbulence in the deep cycle continued to penetrate below the nighttime mixed layer, but the thickness of the region over which the cycle operated decreased as the nighttime mixed layer deepened because the cycle's penetration depth was limited to the region of small Richardson number above the undercurrent core.

4. The turbulent kinetic energy dissipation rate ε at depths between 20 and 80 m decreased by a factor of about 2 ($1.77 \pm 0.66 \times 10^{-7}$ W kg^{-1} to $0.94 \pm 0.25 \times 10^{-7}$ W kg^{-1}). The decrease in dissipation could have been caused by the weaker shear (20- to 100-m averaged shear-squared decreased from $1.72 \pm 0.14 \times 10^{-4}$ W kg^{-1} to $0.57 \pm 0.16 \times 10^{-4}$ W kg^{-1}) and stratification (20- to 100-m averaged N^2 decreased from $0.63 \pm 0.06 \times 10^{-4}$ s^{-2} to $0.23 \pm 0.06 \times 10^{-4} s^{-2}$) and/or the weaker surface wind energy and cooling convection. (The surface wind energy decreased from 0.57 ± 0.10 W m^{-2} to 0.36 ± 0.13 W m^{-2}.) Below 100 m, ε increased.

5. The turbulent thermal dissipation rate χ decreased between 40 and 160 m by more than an order of magnitude (from $5.2 \pm 0.5 \times 10^{-8}$ °C^2 s^{-1} to $0.3 \pm 0.03 \times 10^{-8}$ °C^2 s^{-1}).

6. The Cox number increased at most depths.

7. The vertical heat flux downward from the base of the mixed layer decreased from approximately 40 W m^{-2} (days 1–31 average is 43 ± 5) to less than 10 W m^{-2} on the final day. This heat flux decreased in spite of the increase in turbulent diffusivity because of

the decrease in vertical temperature gradient (to near zero at these depths).

If a decrease in downward heat flux simultaneous with the passage of the downwelling Kelvin wave front is typical at the onset of an El Niño, it could explain the rapid SST increase seen at the onset. The decrease in downward turbulent heat flux would warm the surface water much more quickly than could the advection of warm waters eastward.

In fact, the change in downward turbulent heat flux during the passage of the Kelvin wave was similar in magnitude to the horizontal advection, i.e.,

$$Q_{\text{turb}} \sim \rho C_p \, u' \, T_x \, h$$

where Q_{turb} is the change in vertical turbulent transport as the Kelvin wave passed (30 W m^{-2}), ρC_p is the specific heat per unit volume (4.18×10^6 J $°C^{-1}$ m^{-3}), u' is the change in westward current associated with the Kelvin wave (0.5 m s^{-1}), T_x is the zonal temperature gradient associated with the wave (10^{-6} °C m^{-1}), and h is the depth of the surface layer (30 m).

Acknowledgments. For help at sea aboard R/V *Wecoma* we thank David Hebert, Mary-Elena Carr, Chaojiao Sun, Michael Neeley-Brown, Ed Llewellyn, Ray Kreth, Pat Collier, Mary Mooney, and Vasillis Zervakis. We thank David Hebert also for processing the *Wecoma's* ADCP and meteorological data. The OSU portion of this work was funded by the National Science Foundation (grants OCE 8816098 and OCE 9314396). For help at sea aboard the R/V *Moana Wave* we are indebted to Jack Miller, Earl Krause, Steven Bayer, Lisa Bogar, Dale Hirt, Gordy Welsh, Tom Lehman, and Keith Brainerd. The UW-APL portion of the work was also funded by the National Science Foundation (grants OCE 8815961 and OCE 9316004). We also thank the TOGA-TAO Project Office, Michael J. McPhaden, Director, for providing long term data from the NOAA-PMEL mooring at 0°, 140°W. Paul Freitag and Dai McClurg of NOAA-PMEL provided helpful advice for accessing and processing the long term data. Plate 2 is courtesy of William Kessler of NOAA-PMEL. Discussions with William Kessler and Eric Johnson concerning the nature of the equatorial Kelvin wave were very helpful. Discussions with Hemantha Wijesekera, Keith Brainerd, Harvey Seim, and David Winkel regarding turbulence variability were also helpful.

References

Anis, A., and J. N. Moum, Surface wave-turbulence interactions: Scaling $\epsilon(z)$ near the surface of the ocean, *J. Phys. Oceanogr.*, in press, 1995.

Chereskin, T. K., J. N. Moum, P. J. Stabeno, D. R. Caldwell, C. A. Paulson, L. A. Regier, and D. Halpern, Fine-scale variability at 140°W in the equatorial Pacific, *J. Geophys. Res., 91,* 12,887–12,897, 1986.

Chertock, B., C. W. Fairall, and A. B. White, Surface-based measurements and satellite retrievals of broken cloud properties in the equatorial Pacific, *J. Geophys. Res., 98,* 18,489–18,500, 1993.

Cox, M. D., Generation and propagation of 30-day waves in a numerical model of the Pacific, *J. Phys. Oceanogr., 10,* 1168–1186, 1980.

Crawford, W. R., and T. R. Osborn, Control of equatorial ocean currents by turbulent dissipation, *Science, 212,* 539–540, 1981.

Dillon, T. M., J. N. Moum, T. K. Chereskin, and D. R. Caldwell, Zonal momentum balance at the equator, *J. Phys. Oceanogr., 19,* 561–570, 1989.

Gregg, M. C., H. Peters, J. C. Wesson, N. S. Oakey, and T. J. Shay, Intensive measurements of turbulence and shear in the equatorial undercurrent, *Nature, 318,* 140–144, 1985.

Halpern, D., R. A. Knox, and D. S. Luther, Observations of 20-day period meridional current oscillations in the upper ocean along the Pacific equator, *J. Phys. Oceanogr., 18,* 1514–1534, 1988.

Hebert, D., J. N. Moum, and D. R. Caldwell, Does ocean turbulence peak at the equator?: Revisited, *J. Phys. Oceanogr., 21,* 1690–1698, 1991a.

Hebert, D., J. N. Moum, C. A. Paulson, D. R. Caldwell, T. K. Chereskin, and M. J. McPhaden, The role of the turbulent stress divergence in the equatorial Pacific zonal momentum balance, *J. Geophys. Res., 96,* 7127–7136, 1991b.

Hebert, D., J. N. Moum, C. A. Paulson, and D. R. Caldwell, Turbulence and internal waves at the equator, II, Details of a single event, *J. Phys. Oceanogr., 22,* 1346–1356, 1992.

Johnson, E. S., and M. J. McPhaden, Effects of a three-dimensional mean flow on intraseasonal Kelvin waves in the equatorial Pacific Ocean, *J. Geophys. Res., 98,* 10,185–10,194, 1993.

Kessler, W. S., M. J. McPhaden, and K. M. Weickmann, Forcing of intraseasonal Kelvin waves in the equatorial Pacific, *J. Geophys. Res.*, in press, 1995.

Legeckis, R., Long waves in the eastern equatorial Pacific Ocean: A view from a geostationary satellite, *Science, 197,* 1179–1181, 1977.

Lien, R.-C., M. J. McPhaden, and D. Hebert, Intercomparison of ADCP measurements at 0°, 140°W, *J. Atmos. Oceanic Technol., 11,* 1334–1349, 1994.

Lombardo, C. P., and M. C. Gregg, Similarity scaling of viscous and thermal dissipation in a convecting surface boundary layer, *J. Geophys. Res., 94,* 6273–6284, 1989.

McPhaden, M. J., TOGA-TAO and the 1991–93 El Niño-Southern Oscillation event, *Oceanography, 6,* 36–44, 1993.

McPhaden, M. J., and M. E. McCarty, Mean seasonal cycles and interannual variations at 0°, 110°W and 0°, 140°W during 1980–1991, *Tech. Memo. ERL PMEL 95,* Natl. Oceanic and Atmos. Admin., Silver Spring, Md., 1992.

McPhaden, M. J., and H. Peters, Diurnal cycle of internal wave variability in the equatorial Pacific ocean: Results from moored observations, *J. Phys. Oceanogr., 22,* 1317–1329, 1992.

Moum, J. N., and D. R. Caldwell, Local influences on shear flow turbulence in the equatorial ocean, *Science, 230,* 315–316, 1985.

Moum, J. N., D. R. Caldwell, C. A. Paulson, T. K. Chereskin, and L. A. Regier, Does ocean turbulence peak at the equator?, *J. Phys. Oceanogr., 16,* 1991–1994, 1986.

Moum, J. N., D. R. Caldwell, and C. A. Paulson, Mixing in the equatorial surface layer and thermocline, *J. Geophys. Res., 94,* 2005–2021, 1989.

Moum, J. N., M. J. McPhaden, D. Hebert, H. Peters, C. A. Paulson, and D. R. Caldwell, Internal waves, dynamic instabilities, and turbulence in the equatorial thermocline: An introduction to three papers in this issue, *J. Phys. Oceanogr., 22,* 1357–1359, 1992a.

Moum, J. N., D. Hebert, C. A. Paulson, and D. R. Caldwell, Turbulence and internal waves at the equator, I, Statistics from towed thermistors and a microstructure profiler, *J. Phys. Oceanogr., 22,* 1330–1345, 1992b.

Moum, N. J., M. C. Gregg, R.-C. Lien, and M.-E. Carr, Comparison of turbulence, kinetic energy dissipation rate estimates from two ocean microstructure profilers, *J. Atmos. Ocean Tech., 12,* 346–366, 1995.

Osborn, T. R., Estimates of the local rate of diffusion from dissipation measurements, *J. Phys. Oceanogr., 10,* 83–89, 1980.

Peters, H., M. C. Gregg, and J. M. Toole, On the parameterization of equatorial turbulence, *J. Geophys. Res., 93,* 1199–1218, 1988.

Peters, H., M. C. Gregg, and J. M. Toole, Meridional variability of turbulence through the equatorial undercurrent, *J. Geophys. Res., 94,* 18,003-18,009, 1989.

Peters, H., M. C. Gregg, and T. B. Sanford, Equatorial and off-equatorial fine-scale and large-scale shear variability at 140°W, *J. Geophys. Res., 96,* 16,913–16,928, 1991.

Peters, H., M. C. Gregg, and T. B. Sanford, The diurnal cycle of the upper equatorial ocean: Turbulence, fine-scale shear, and mean shear, *J. Geophys. Res., 99,* 7707–7723, 1994.

Philander, S. G. H., Instabilities of zonal equatorial currents, 2, *J. Geophys. Res., 83,* 3679–3682, 1978.

Philander, S. G. H., and R. C. Pacanowski, The generation of Equatorial Currents, *J. Geophys. Res., 85,* 1123–1136, 1980.

Ramage, C. S., El Niño, *Sci. Am., 254*(6), 77–84, 1986.

Toole, J. M., H. Peters, and M. C. Gregg, Upper ocean shear and density variability at the equator during TROPIC HEAT, *J. Phys. Oceanogr., 17,* 1397–1406, 1987.

Wunsch, C., and A. E. Gill, Observations of equatorially trapped waves in Pacific sea level variations, *Deep Sea Res., 23,* 371–390, 1976.

Wyrtki, K., and B. Kilonsky, Mean water and current structure during the Hawaii-to-Tahiti Shuttle Experiment, *J. Phys. Oceanogr., 14,* 242–254, 1984.

D. R. Caldwell and J. N. Moum, College of Oceanic and Atmospheric Sciences, Oregon State University, Oceanography Administration Building 104, Corvallis, OR 97331. (e-mail: caldwell@oce.orst.edu; moum@oce.orst.edu)

M. C. Gregg and R.-C. Lien, Applied Physics Laboratory, University of Washington, Seattle, WA 98105.

(Received July 5, 1994; revised September 26, 1994; accepted December 13, 1994.)